[CANCER RESEARCH 64, 6924–6933, October 1, 2004]

Inhibition of gp130 Signaling in Breast Cancer Blocks Constitutive Activation of Stat3 and Inhibits *in Vivo* Malignancy

Katri S. Selander,[1] Li Li,[1] Latania Watson,[1] Melinda Merrell,[1] Heike Dahmen,[3] Peter C. Heinrich,[3] Gerhard Müller-Newen,[3] and Kevin W. Harris[1,2]

[1]Department of Medicine, Division of Hematology/Oncology, University of Alabama at Birmingham, Birmingham, Alabama; [2]Birmingham Veterans Affairs Medical Center, Birmingham, Alabama; [3]Institut für Biochemie, Universitätsklinikum Rheinisch-Westfälische Technische Hochschule Aachen, Aachen, Germany

ABSTRACT

The cytokine receptor gp130 is the common signaling subunit of receptors used by the interleukin (IL)-6 cytokine family. gp130 is widely expressed in breast cancer cell lines and primary tumors. The role of gp130 in breast cancer *in vivo* is unknown. To study the effect of gp130 inhibition in breast cancer, endogenous gp130 signaling in breast cancer cell lines was blocked with a dominant-negative gp130 protein (DN gp130). DN gp130 inhibited constitutive Stat3 activation in breast cancer cells. Both gp130 and epidermal growth factor receptor (EGFR) have been implicated in constitutive Stat3 activation in breast cancer. There are known physical and functional interactions between gp130 and EGFR. Consistent with this, we show that DN gp130 inhibits signaling downstream of the EGFR in breast cancer cells. The effect of DN gp130 on breast cancer *in vivo* was assessed with an orthotopic nude mouse model. DN gp130 MDA-231 cells had markedly decreased engraftment, size, and metastasis compared with control cells. These results are particularly striking considering that DN gp130-expressing breast cancer cells grow faster *in vitro*. We hypothesized that DN gp130 expression results in inhibition of invasion and metastasis *in vivo*. Marked angiogenesis was present in tumors from control animals and was absent in tumors from DN gp130 animals. We additionally show that tissue inhibitor of metalloproteinase-3, an inhibitor of tumor invasion and angiogenesis, is upregulated in both MDA-231 DN gp130 cells and tumors. These results, in light of the availability of several potential pharmacological inhibitors of gp130, suggest novel approaches to breast cancer therapy.

INTRODUCTION

The cytokine receptor gp130 is the common signaling subunit for the interleukin (IL)-6 family of cytokines. The gp130 is ubiquitously expressed in tissues and mediates numerous homeostatic functions, including immune response, inflammation, bone metabolism, and hematopoiesis (1). IL-6, IL-11, oncostatin M, leukemia inhibitory factor, and ciliary neurotropic factor are among the IL-6 family cytokines that use gp130 as a signaling subunit. The functional oligomeric receptors for these cytokines also include at least one other ligand-specific binding subunit. All of the IL-6 cytokines require gp130 for biologically functional signaling (2).

After ligand binding, gp130 supports activation of the receptor-associated tyrosine kinases Jak1, Jak2, and Tyk2 for initial signal transduction (2). Jak activation leads to activation of downstream signaling pathways, including phosphatidylinositol 3′-kinase, and mitogen-activated protein kinases. An important target of gp130 signaling is Stat3 (3, 4). Stat3 is a member of the Stat family of latent cytoplasmic transcription factors. After gp130 activation, Stat3 becomes tyrosine phosphorylated, homo- or heterodimerizes, and translocates to the nucleus where it induces gene transcription. Stat3 transcriptionally activates numerous important cellular genes involved in growth regulation, differentiation, and cell cycle, including c-myc and bcl-2 (3).

Stat3 is an oncogene (5). Constitutive Stat3 activation is found in numerous solid tumors including breast cancer (6). Constitutive activation of Stat3 is required for the transformed phenotype of tumor-derived breast cancer cell lines (6). Thus, Stat3 seems to be a central mediator of breast malignancy. Several groups have studied the molecular basis for the constitutive activation of Stat3 in breast cancer. Epidermal growth factor (EGF) signaling is important in this process (7–9). Signaling through gp130 supports constitutive activation in Stat3 in head and neck cancer (10). gp130 may have a similar activity in breast cancer because inhibition of Jak2 results in inhibition of constitutive Stat3 activation in breast cancer (7, 11). c-Src is also involved in Stat3 activation in breast cancer cells (9, 11).

gp130 is expressed in the majority of breast cancer cell lines (12) and in most primary breast cancer tumors (12, 13). gp130 expression in primary breast tumors (as assessed by reverse transcription-PCR; RT-PCR) was found to be associated with good prognosis in one study (13).

gp130 ligands have numerous reported biological effects on breast cancer cells. IL-6, oncostatin M, and leukemia inhibitory factor have been shown to induce differentiation and growth inhibition of breast cancer cells. For instance, oncostatin M can support differentiation of breast cancer cells as assessed by morphology and the expression of differentiation markers (14). IL-6 and oncostatin M induce disruption of cell adhesion and increased motility of breast cancer cells (15, 16). IL-6 has also been reported to activate the estrogen receptor in breast cancer cells (17).

Interestingly, gp130 has been found to physically and functionally interact with EGFR family members. IL-6 induces tyrosine phosphorylation of erbB-2 in a prostate cancer cell line (18). gp130 and erbB-2 form an IL-6 dependent complex in prostate cancer cells. Apparently, this interaction is required for full IL-6 activity. The interaction of gp130 and EGFR family members also occurs in breast cancer cells. For instance, EGFR is required for full signaling activity of IL-6 in T-47D breast cancer cells (15). Similar results were obtained in studies on oncostatin M signaling in breast cancer cells (19). In these experiments, both gp130 and the related receptor oncostatin M receptor β were found to be physically associated with erbB-2 and erbB-3. This interaction supports EGF-induced tyrosine phosphorylation of gp130.

The molecular mechanism and biological significance of the gp130/EGFR interactions are incompletely understood. The effect of specific inhibition of gp130 signaling on breast cancer activity *in vitro* has not been reported previously. More importantly, there are no published studies involving manipulation of gp130 in breast cancer *in vivo*.

The diverse reported activities of gp130 ligands on breast cancer cells make it difficult to predict the overall effect of gp130 signaling

Received 8/13/03; revised 6/24/04; accepted 8/3/04.

Grant support: VA Merit Award (K. Harris), UAB Breast SPORE pilot project grant (K. Harris), Avon Grant (K. Selander), UAB Center for Metabolic Bone Disease pilot project Grant (K. Selander), the Deutsche Forschungsgemeinschaft, and the Fonds der Chemischen Industrie.

The costs of publication of this article were defrayed in part by the payment of page charges. This article must therefore be hereby marked *advertisement* in accordance with 18 U.S.C. Section 1734 solely to indicate this fact.

Note: K. S. Selander, L. Li, and L. Watson contributed equally to this article.

Requests for reprints: Kevin W. Harris, University of Alabama at Birmingham, Division of Hematology/Oncology, WTI 520-D, 1530 3rd Avenue South, Birmingham, Alabama 35294-3300; Phone: (205) 934-6995; Fax: (205) 975-6911; E-mail: kevin.harris@ccc.uab.edu.

in breast cancer *in vivo*. The need to determine the importance of gp130 signaling in breast cancer is compelling because specific pharmacological inhibition of gp130 signaling is feasible (20, 21). To address this issue, we have prepared and characterized breast cancer cells in which endogenous gp130 signaling is inhibited.

MATERIALS AND METHODS

Materials. Oncostatin M and AG1478 were obtained from Calbiochem (San Diego, CA). EGF antibody was obtained from R&D Systems (Minneapolis, MN). The gp130 monoclonal antibodies B-S12 and B-P4 were obtained from Diaclone (Canton, MA). ErbB-2 phosphospecific antibody was obtained from Upstate (Waltham, MA). Jak2 phosphospecific antibody was obtained from Biosource (Camarillo, CA). Shc phosphospecific antibody was from Calbiochem. CD31 antibody was from NeoMarkers (Fremont, CA). All of the other primary antibodies were from Santa Cruz Biotechnology (Santa Cruz, CA). Secondary antibodies labeled with horseradish peroxidase were obtained from Pierce (Rockford, IL) and Cell Signaling (Beverly, MA).

Cell Lines. Parental MDA- 231 cells were cultured in complete DMEM (supplied with 1% nonessential amino acid solution) from Cellgro (Herndon, VA) containing 10% heat-inactivated FCS. SKBR3 cells were cultured in DMEM/F12 containing 10% heat-inactivated FCS. T-47D cells were grown in RPMI (phenol red-free) with 10% FCS supplemented with insulin. COS-7 cells and HepG2 cells were cultured in DMEM and DMEM/F12, respectively, in the presence of 10% heat-inactivated FCS. For the measurement of cell growth, 1×10^3 cells were cultured per well in 100 μL of complete DMEM on 96-well plates. Cells were assayed in quadruplicate. The assay was done with the CellTiter 96 Aqueous One Solution Cell Proliferation Assay from Promega (Madison, WI).

Vector Construction and Transfection of Cells. The plasmid pSVLgp-130Δcyt was constructed with the vector pSVLgp130 containing the human full-length gp130 cDNA by deleting the sequence encoding the COOH-terminal 282 amino acids of gp130. For reporter gene assays in HepG2 cells, gp130Δcyt was subcloned into the expression vector pRc/CMV. The pcDNA3.1-DN gp130 was constructed by subcloning of the 1.9-kb DN gp130 fragment from pSVL gp130Δcyt into the *Xho*I/*Bam*HI sites of pcDNA3.1-(Invitrogen, Carlsbad, CA). Transfection of MDA-231 and SKBR3 cells with pcDNA3.1-DN gp130 was done with TransIT-Express Transfection Reagent (Mirus, Madison, WI). Stably transfected cells were selected in the presence of G418 (0.6 mg/ml) and then subsequently single-cell cloned in 96-well plates with the limited dilution method. Single-cell clones were subsequently maintained in 0.4 mg/ml G418. Expression of DN gp130 mRNA in cell lines was verified with RT-PCR.

RT-PCR and RNase Protection Assay. Total RNA was isolated by TRIzol reagent (Invitrogen), as described by the manufacturer. Transfected cell lines were examined for expression of gp130Δcyt mRNA by RT-PCR. Primers that specifically recognize a 200-bp RT-PCR product from the transfected mutant gp130 gene were designed. The primers were as follows: 5′ primer 5′GCT AGC GTT TAA ACG GGC CCT CTA3′ (from pcDNA3.1-sequence) and 3′ primer 5′ CCT TTA GCA CAC AAA CTG CAG TGA 3′ (from DN gp130 sequence). RNase protection assay was done with a commercial *in vitro* transcription and nonradioactive detection kit from BD Biosciences (San Diego, CA). A commercial multiprobe template set was used (hMMP-1 probe set from BD Biosciences).

Electromobility Shift Assay. COS-7 cells were transfected with the DEAE-dextran method. COS-7 cells grown in a 10-cm Petri dish to 80 to 100% confluency were washed twice with PBS. The cells were incubated for 80 minutes with the transfection mixture consisting of 7.5 ml FCS-free medium, 60 μL DEAE-dextran (50 mg/ml; Amersham Pharmacia Biotech, Uppsala, Sweden), 20 μg plasmid DNA (either 20 μg of pSVL empty vector or 4 μg of pCDM8-IL-6Rα and 16 μg of pSVL empty vector or 4 μg of pCDM8-IL-6Rα and 16 μg of pSVLgp130Δcyt or as indicated in Fig. 1*E*), and 6 μL chloroquine (100 mmol/L; Sigma, Taufkirchen, Germany). Plasmid DNA concentrations were optimized to obtain the best dominant-negative effect. Subsequently, cells were washed with PBS and incubated with 6 ml 10% DMSO in PBS for 1 minute. After an additional PBS washing step, the cells were supplied with culture medium. The experiments were done 48 hours after transfection. Cells were stimulated with IL-6 for 15 minutes, and then nuclear extracts were prepared. STAT DNA-binding activity was determined by an electrophoretic mobility shift assay with the m67SIE-probe derived from the c-fos promoter (5′-GATCC GGGAG GGATT TACGG GAAAT GCTG-3′). Protein/DNA complexes were detected by autoradiography with a PhosphorImager (Storm 840, Molecular Dynamics, Sunnyvale, CA).

HepG2 Cell Stat3 Reporter Gene Assay. HepG2 cells were transfected with the gp130Δcyt construct, the reporter plasmid pGL3 127 1ACT, and pCR3LacZ with the calcium phosphate precipitation method. Twenty micrograms plasmid DNA (0.5 μg/μL) were mixed with 62 μL 2 M $CaCl_2$. After addition of 0.5 ml of 40 mmol/L HEPES, 274 mmol/L NaCl, 10 mmol/L KCl, 1.4 mmol/L Na_2HPO_4, and 100 mmol/L glucose, the DNA-calcium precipitate was suspended with 10 ml medium and added to the cells on a 10-cm Petri dish. After incubation for 12 hours, the cells were washed with PBS and transferred to standard growth medium. Twenty-four hours after transfection, cells were stimulated with IL-6 for 12 hours. Subsequently, cells were lysed, and luciferase activity was measured with the Luciferase Assay System with Reporter Lysis Buffer Kit (Promega) as described by the manufacturer. Luminescence was measured with a Microlumat 96P (EG&G Berthold, Bad Wildbach, Germany). All of the luciferase values were standardized for transfection efficiency by measuring β-galactosidase activity because of expression of the pCR3LacZ plasmid.

Western Blots. COS-7 cells were transfected with 20 μg of the respective plasmid. Forty-eight hours after transfection, cells of a 10-cm Petri dish were washed once with cold PBS and lysed with 1 ml radioimmunoprecipitation assay lysis buffer supplemented with protease inhibitors. For immunoprecipitation, 1 μg of the Diaclone antibody B-S12 was added and incubated at 4°C for at least 6 hours. Immunocomplexes were precipitated with 5 mg protein A-Sepharose (Amersham) that was preincubated with a rabbit antimouse antibody (4 μg/10 mg). Bound proteins were released by incubation with 30 μL of 2× Laemmli probe buffer for 5 minutes at 95°C. Released proteins were separated by SDS-PAGE and analyzed by Western blot with the Diaclone antibody B-P4. Breast cancer cells were studied at 80% confluence on 100-mm Petri dishes. For stimulation studies, cells were starved overnight in serum-free media. Cells were then simulated with EGF (10 ng/ml) or oncostatin M (2 ng/ml) for 15 minutes and then lysed. Cells were lysed with Cell Lysis Buffer (Cell Signaling), supplemented with 1 mmol/L phenylmethylsulfonyl fluoride, 1 mmol/L sodium vanadate, and 1:100 dilution of Protease Inhibitor Cocktail Set III (Calbiochem). Cells were lysed for 15 minutes on ice in 200 μL of lysis buffer. Lysates were centrifuged at 15,000 rpm for 15 minutes in the cold. Protein concentration of each sample was determined with the DC Protein Assay from Bio-Rad (Hercules, CA). We used the smallest protein value (range 80 to 160 μg) to normalize the protein concentrations of all samples on a gel. Samples were electrophoresed on 12% SDS minigels and transferred to nitrocellulose. Densitometry was done with NIH image analysis software.

Matrigel Invasion Assay. Breast cancer cells were plated on the upper wells of Matrigel invasion chambers (Becton Dickinson, Bedford, MA) at a density of 0.5×10^5 cells/500 μL in normal culture medium containing 2% FCS. Medium containing 10% FCS was applied to the lower chamber as a chemoattractant to induce invasion, according to the manufacturer's instructions. The cells were incubated for 18 hours at 37°C and 5% CO_2, and the insert membranes were then prepared for microscopic samples. Membranes were fixed and stained with the HEMA 3 stain set (Fisher Scientific, Hampton, NH). The cells on the upper surface of the membrane were wiped off with cotton wool, the membranes were then cut from the inserts, and the membranes were mounted with glycerol-PBS (1:9). The number of cells on the lower surface of the membrane was counted by microscope (×50 objective) from 5 consecutive fields. Each treatment was done in quadruplicate.

Flow Cytometry of Breast Cancer Cells for Cell Surface Expression of gp130. Cells were centrifuged and rinsed once with cold PBS/5% FCS. Cells were resuspended in 100 μL PBS/5% FCS and 1 μg of gp130 extracellular domain B-P4 antibody was added. Cells were incubated for 20 minutes on ice and washed with PBS/5% FCS. For detection of bound antibodies a 1:50 or 1:100 dilution of a PE-conjugated goat-antimouse IgG, (Fab')2-fragment was used (BD Bioscience). Cells were incubated with the secondary antibody for 30 minutes in the dark on ice. Cells were washed again with PBS/5% FCS and resuspended in PBS/5% FCS for flow cytometric analysis.

Mouse Mammary Fat Pad Assay. All of the animal research procedures were approved by our institutional animal care and use committee before animal experimentation. Various single-cell clones of MDA-231 transfectants

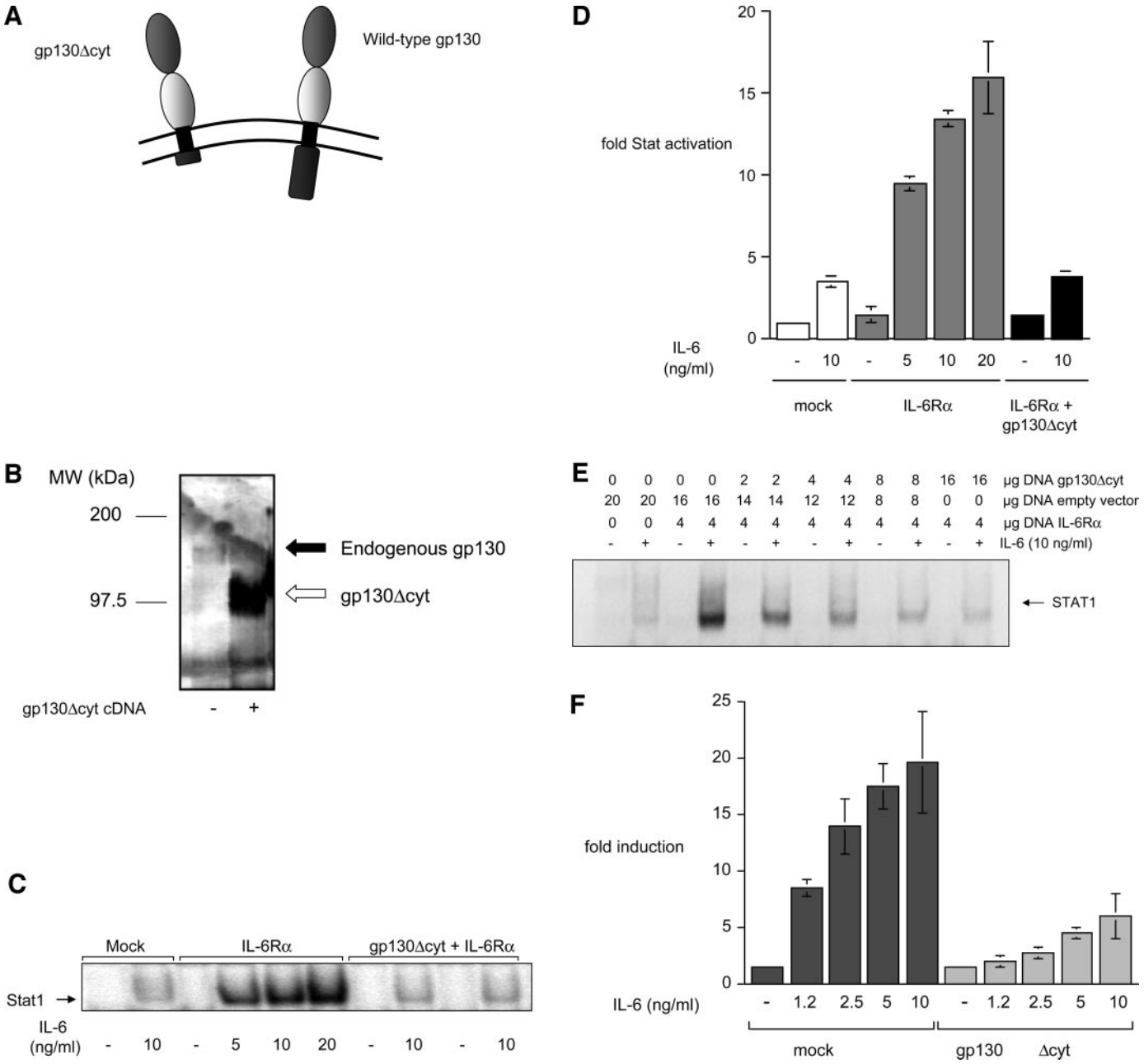

Fig. 1. gp130Δcyt acts as a dominant-negative gp130 protein. *A*, structure of the gp130Δcyt and gp130 wild-type proteins. *B*. COS-7 cells were transiently transfected with mock vector (*left lane*) or an expression vector encoding gp130Δcyt. The gp130 protein was immunoprecipitated from total cell lysates with the B-S12 antibody and immunoblotted with the antibody B-P4. Both antibodies recognize the gp130 extracellular domain. The bands representing endogenous wild-type gp130 and gp130Δcyt are indicated by *arrows*. *C*, dominant-negative effect of gp130Δcyt on STAT activation in COS-7 cells. COS-7 cells were transfected with pSVL empty vector (Mock, 20 μg of DNA), with pCDM8-IL-6Rα (4 μg of DNA) and pSVL empty vector (16 μg of DNA), or with pCDM8-IL-6Rα (4 μg of DNA) and pSVLgp130Δcyt (16 μg of DNA). Forty-eight hours after transfection, cells were stimulated with various amounts of IL-6 for 15 minutes as indicated. Nuclear extracts were prepared and analyzed for STAT-DNA binding with the [^{32}P]-labeled, double-stranded m67SIE-probe. Protein/DNA-complexes were separated by gel-electrophoresis and detected by autoradiography. The STAT-signals in the electrophoretic mobility shift assay were quantified with a phosphorimager (*D*). The values are derived from four independent experiments; *bars*, ±SD. *E*. Inhibition of STAT activation is gp130Δcyt dose-dependent. COS-7 cells were transfected with a constant amount of IL-6Rα and increasing amounts of gp130Δcyt expression vectors as indicated in the figure. Forty-eight hours after transfection, cells were stimulated with 10 ng/ml of IL-6 for 15 minutes. STAT1 activation was detected in a gel shift assay as described in *C* above. *F*, dominant-negative effect of gp130Δcyt on *α1ACT* gene induction in HepG2 cells. HepG2 cells were transfected with a reporter gene construct (pGL3α1ACT), a β-galactosidase-expression plasmid (pCR3LacZ), and pRC/CMV-empty vector or pRC/CMVgp130Δcyt (ratio 1:1.2:18). Thirty-six hours after transfection, cells were stimulated for 12 hours with various amounts of IL-6 as indicated. Subsequently, cells were lysed, and luciferase and galactosidase activities (as a normalization control) were measured. The *bars* show fold luciferase induction compared with unstimulated cells. Values of three independent experiments; *bars*, ±SD. (*MW*, molecular weight)

(10^6 cells in 100 μL of sterile PBS) were inoculated locally into the mammary fat pads of 4- to 6-week-old female athymic nude mice (Taconic Farms, Germantown, NY), with a 27.5 G needle. Either one or two sites per mouse were injected. Tumors were allowed to form for 28 days, after which the mice were sacrificed, and the locally formed tumors were excised. Tumor dimensions were measured with a caliper, and the tumor volumes were calculated with the formula $V = (\pi/6)(d_1 \times d_2)^{3/2}$ (22). Some tumors were fixed in 10% neutral-buffered formalin for 24 hours and processed routinely into paraffin blocks. Tumor rate of engraftment (defined as a measurable tumor) and size was expressed as mean ± SD. Student's *t* test was used to determine the p value. A p value of <0.05 was considered statistically significant.

Immunohistochemical Staining. Histologic sections of 5 microns were cut from paraffin blocks of tumors with a microtome and processed for immunohistochemical detection of CD31, an endothelial cell marker (23), or

tissue inhibitor of metalloproteinase (TIMP)-3. Appropriate positive and negative controls were used to ensure good histochemical staining. Apoptotic nuclei were detected from histologic sections of the paraffin-embedded tumors, with a terminal deoxynucleotidyl transferase-mediated nick end labeling (TUNEL)-method, and the *In situ* Cell Death Detection Kit (Roche, Indianapolis, IN) was used, according to the manufacturer's instructions. We used a 100× objective to count the number of apoptotic nuclei from 6 random fields per section, with fluorescent microscope.

RESULTS

gp130Δcyt Acts as a Dominant-Negative Inhibitor of gp130 Signaling. To block endogenous gp130 signaling in breast cancer cells, we constructed a gp130 cytoplasmic truncation mutant (gp130Δcyt) that lacks all but 6 amino acids of the cytoplasmic domain (Fig. 1*A*). This truncated gp130 is unable to support normal gp130 signal transduction, because the signaling motifs of the cytoplasmic domain are completely deleted (2). Because gp130Δcyt retains the extracellular and transmembrane domains, it is still able to interact with its cell surface binding partners (such as IL-6R α). Thus, we hypothesized that gp130Δcyt should act as a dominant-negative inhibitor of gp130 signaling. On overexpression in transiently transfected COS-7 cells, gp130Δcyt can be clearly detected in Western blot (Fig. 1*B*). The activation of Stat1 in response to IL-6 was studied in COS-7 cells transfected with either IL-6R α, IL-6R α + gp130Δcyt, or vector-only (Fig. 1, *C* and *D*). Gel shift assays were done to detect STAT1 activation. Stat3 is only weakly activated in response to IL-6 in COS-7 cells (data not shown). The IL-6-induced Stat1-DNA complex formation is markedly decreased by overexpression of gp130Δcyt. The inhibition of IL-6 signaling depends on the amount of transfected gp130Δcyt plasmid (Fig. 1*E*).

IL-6 treatment of Hep-G2 cells results in the induction of acute phase proteins such as α1-antichymotrypsin (α1ACT; ref. 24). Stat3 is the major transcription factor involved in the induction of acute phase protein genes (25). We tested the ability of gp130Δcyt to inhibit the activation of the α1ACT promoter after IL-6 treatment of HepG2 cells (Fig. 1*F*). A luciferase reporter construct containing the α1ACT promoter was cotransfected into HepG2 cells with and without a gp130Δcyt expression plasmid. IL-6 treatment led to a dose-dependent activation of the α1ACT promoter in these cells. In the presence of gp130Δcyt protein a marked attenuation of the α1ACT promoter activation was observed, as a result of gp130Δcyt inhibition of endogenous gp130 signaling. Thus, gp130Δcyt acts as a dominant negative inhibitor of gp130 signaling complex. Therefore, we refer to gp130Δcyt as DN gp130 in this report.

Expression of DN gp130 Is Associated with Increased Growth of Breast Cancer Cells *In vitro*. DN gp130 was used to assess the effect of inhibition of gp130 signaling on breast cancer cells. MDA-231 and SKBR3 breast cancer cell lines were used for these experiments. DN gp130 cDNA was stably transfected into each parental cell line. G418 was used to select stable transfectants. Control transfections were done with empty vector cDNA. Several single cell clones of both DN gp130 and control MDA-231 transfectants were additionally studied. We were unable to isolate single cell clones of SKBR3

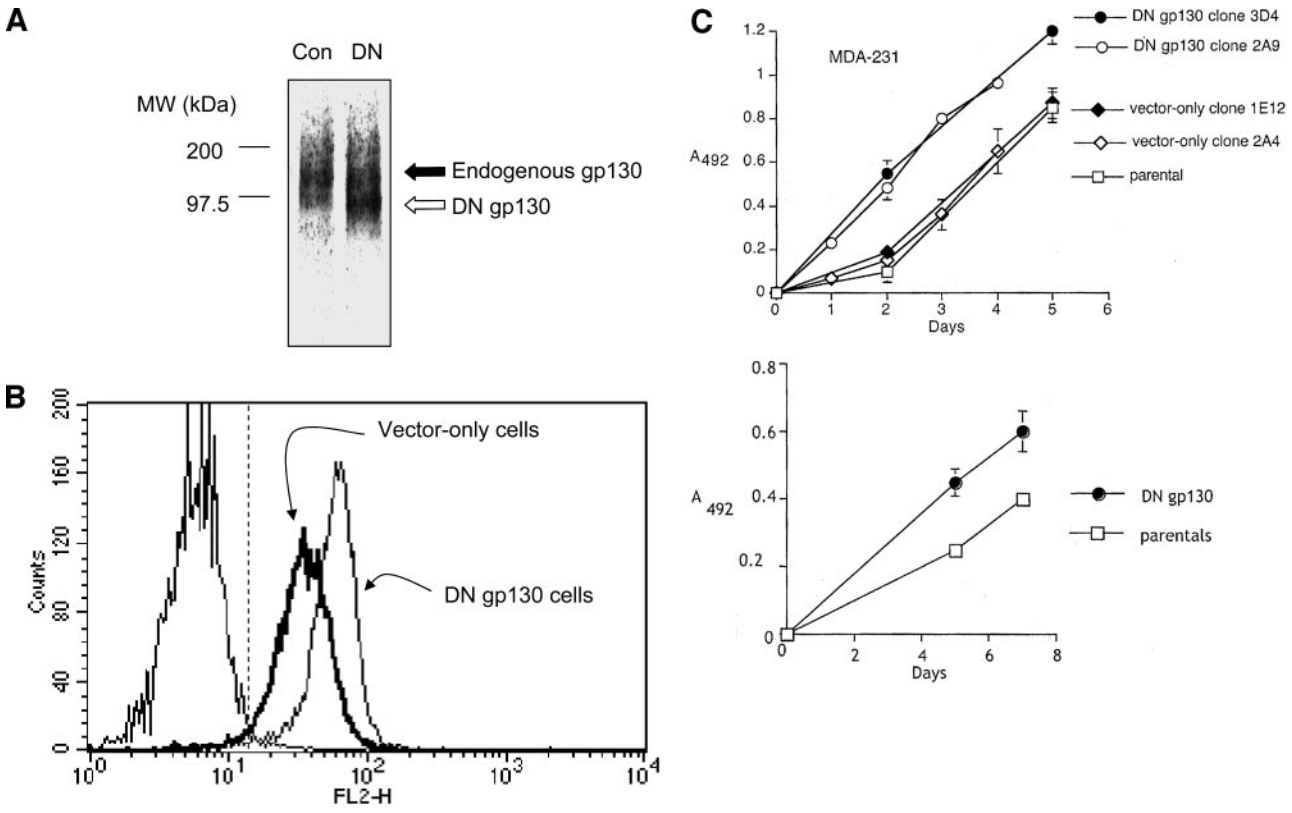

Fig. 2. Cell surface expression of DN gp130 protein increases the growth rate of breast cancer cells. *A*, Western blot of DN gp130 protein in MDA-231 cells. Whole cell lysates of cells at 80% confluence were obtained and electrophoresed on 7.5% SDS gels. *Con*, vector-only control cells. *DN*, cells transfected with DN gp130 cDNA. *Arrows*, the migration of endogenous wild-type gp130 and transfected DN gp130. *B*, flow cytometry of MDA-231 transfectants. Cells in suspension were labeled with anti-gp130 extracellular domain antibody and analyzed by flow cytometry. The population of cells to the left of the *dotted line* indicates nonspecific background staining in the absence of primary antibody. At least 10,000 cells were analyzed for each measurement. Similar results were seen with several independent single-cell clones of vector-only and DN gp130 cells. *C*, Breast cancer cells (5×10^3) were plated in 96-well plates. We assessed cell growth at the indicated time points by using a 3-(4,5-dimethylthiazol-2-yl)-2,5-diphenyltetrazolium bromide assay. MDA-231 cells were various single-cell clones or parentals as indicated. SKBR3 transfected cells were pooled cells. Each point is the average of 4 replicates with SDs shown. In some cases the deviation bars are too small to be visible. (*MW*, molecular weight)

cells containing either DN gp130 or vector-only cDNA, so pools of stably transfected SKBR3 cells were used in these experiments.

DN gp130 protein expression in cells was shown by Western blot (Fig. 2*A*). We used flow cytometric analysis of gp130 in intact cells (Fig. 2*B*) to assess the relative cell surface expression of DN gp130 compared with endogenous wild-type gp130. For instance, in the experiment shown in Fig. 2*B*, mean fluorescence intensity was 1,407 for the DN gp130 clone, and 761 for the vector-only control clone. Because the gp130 extracellular domain antibody detects both DN gp130 and wild-type gp130, we infer that there are approximately equal amounts of endogenous wild-type gp130 and transfected DN gp130 protein expressed on the cell surface of MDA-231 DN gp130 single cell clones. Similar results were seen with other MDA-231 single-cell clones (data not shown).

Inhibition of gp130 was associated with increased cell growth rate of MDA-231 and SKBR3 cells, as shown in Fig. 2*C*. The single cell clones of MDA-231 DN gp130 cells grow at a markedly faster rate than either the control single cell clones or parental MDA-231 cells. Similar results are also seen with SKBR3 cells. Results similar to those in Fig. 2 were obtained from manual cell counts with a hemacytometer (data not shown). These results are consistent with the reported inhibitory effects of gp130 signaling on breast cancer cell growth (15, 19).

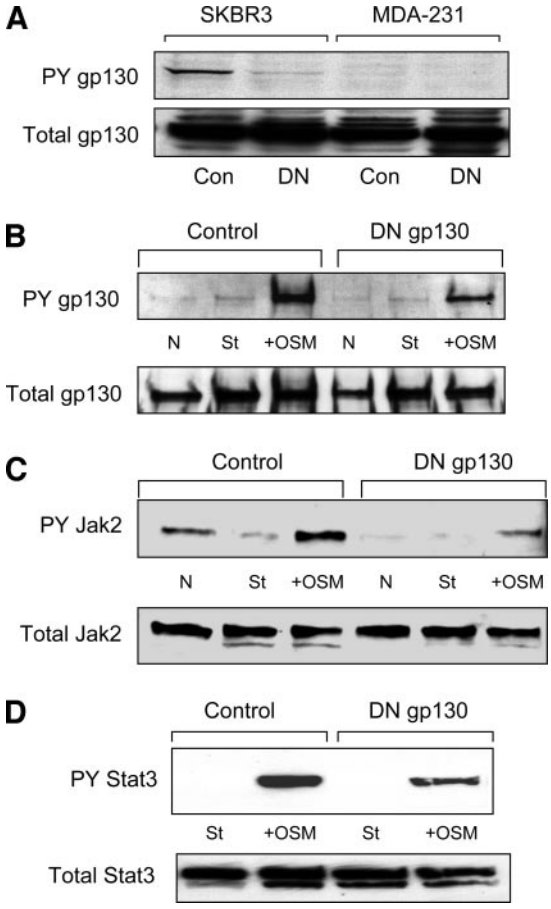

Fig. 3. Inhibition of gp130 signaling in breast cancer cells expressing DN gp130. *A*. SKBR3-transfected pools or MDA-231 single-cell clones were lysed at 80% confluence and immunoblotted with a phosphotyrosine-specific gp130 antibody. *Con*, vector-only control cells. *DN*, DN gp130-expressing cells. The blots were stripped and reblotted with antibody to the gp130 cytoplasmic domain to show equal loading of endogenous wild-type gp130. *B*. MDA-231 single-cell clones expressing either DN gp130 or vector-only control were lysed at steady state growth (*N*), after overnight starvation under serum-free conditions (*St*), or starved and stimulated for 15 minutes with 10 ng/ml of oncostatin M (+*OSM*). Lysates were immunoblotted with a phosphospecific gp130 antibody and then stripped and reblotted with cytoplasmic gp130 antibody to show equal loading. *C*. MDA-231 single-cell clones expressing either DN gp130 or vector-only control were lysed after treatment with oncostatin M as described above. Lysates were immunoblotted with a phosphospecific Jak2 antibody and then stripped and reblotted with total Jak2 to show equal loading. *D*. MDA-231 single-cell clones expressing either DN gp130 or vector-only control were lysed after treatment with oncostatin M as described above. Lysates were immunoblotted with a phosphospecific Stat3 antibody and then stripped and reblotted with total Stat3 to show equal loading. (*PY*, phosphotyrosine)

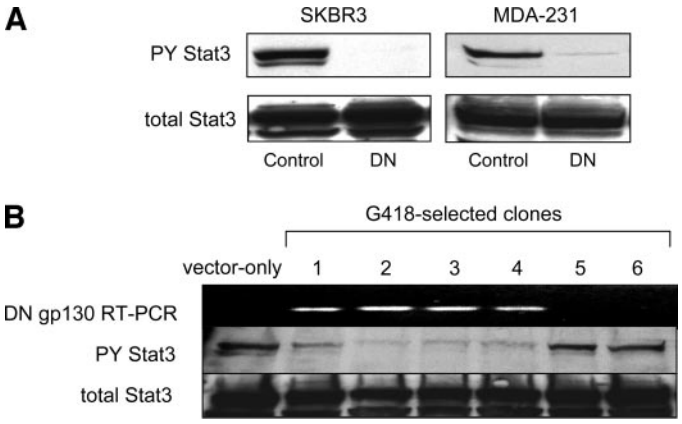

Fig. 4. Expression of DN gp130 in breast cancer cells is associated with inhibition of constitutive Stat3 activation. *A*. SKBR3-transfected pooled cells or MDA-231 single-cell clones were grown to 80% confluence and then lysed and immunoblotted with a phosphotyrosine-specific Stat3 antibody (*PY Stat3*). Blots were stripped and reblotted with antitotal Stat3 to show equal loading. *B*. The expression of DN gp130 mRNA in MDA-231 single-cell clones selected for G418 resistance was determined with RT-PCR. Six single-cell clones transfected with DN gp130 DNA and one single-cell clone transfected with vector-only DNA were studied at 80% confluence. DN gp130 clones #5 and #6 are false-positive clones because no expression of DN gp130 mRNA was detectable by RT-PCR. Phosphotyrosine-specific Stat3 immunoblot demonstrates that the false-positive clones lack inhibition of constitutive Stat3 activation. Blots were stripped and reblotted with a Stat3 antibody to show equal loading.

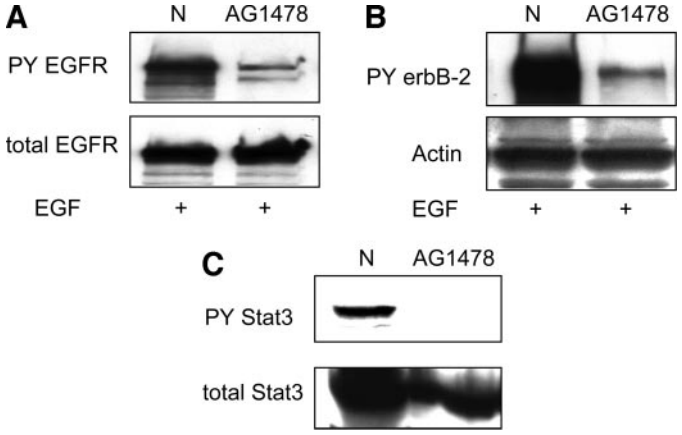

Fig. 5. Inhibition of EGFR signaling in parental MDA-231 cells results in downregulation of constitutive Stat3 activation. MDA-231 parental cells were treated with DMSO vehicle (*N*) or the EGFR inhibitor AG1478 (250 nmol/L) overnight at 37°C. *A*. Cells were stimulated with EGF (10 ng/ml) for 15 minutes and blotted to detect EGF-induced EGFR activation with a phosphospecific EGFR antibody. Blots were stripped and reblotted with EGFR antibodies to show equal loading. *B*. Cells were stimulated with EGF (10 ng/ml) for 15 minutes and blotted to detect EGF-induced erbB-2 activation with a phosphospecific erbB-2 antibody. The blots were stripped and reblotted with antiactin to show equal loading. *C*. Unstimulated cells at 80% confluence were treated with AG1478 as described above. Constitutive Stat3 activation was assessed by Western blot analysis of cell lysates with phosphospecific Stat3 antibodies. Blots were stripped and reblotted with total Stat3 antibodies to show equal loading.

DN gp130 Inhibits gp130 Signaling in Breast Cancer Cells. We verified that DN gp130 inhibits endogenous gp130 signaling in breast cancer cells. Constitutive gp130 activation was detected in SKBR3 cells (Fig. 3*A*). Expression of DN gp130 resulted in a decrease in the constitutive activation of gp130 in these cells. In MDA-231 cells, on the other hand, constitutive gp130 activation is not detected. Treat-

ment of MDA-231 cells with the gp130 ligand oncostatin M results in gp130 activation (Fig. 3*B*). This activation is decreased in DN gp130 expressing MDA-231 cells. Activation of Jak2 and Stat3 in response to oncostatin M stimulation are also blunted in the MDA-231 single-cell clones expressing DN gp130 (Fig. 3, *C* and *D*). These results show a suppression of both constitutive and exogenous ligand-induced gp130 signaling by DN gp130 protein in breast cancer cells.

DN gp130 Inhibits Constitutive Stat3 Activation in Breast Cancer Cells. Constitutive Stat3 activation is an important pathobiologic feature of many solid tumors, including breast cancer. We wondered if inhibition of gp130 signaling has an effect on constitutive Stat3 activation in breast cancer cells. In both SKBR3 and MDA-231 cells constitutive activation of Stat3 is detectable (Fig. 4*A*). This constitutive Stat3 activation is dramatically reduced in the presence of DN gp130. To verify the association of gp130 expression and Stat3 down-regulation, we took advantage of the fact that false positive single cell clones occasionally occur during G418 selection. As shown in Fig. 4*B*, only the "true positive" clones that express DN gp130 mRNA (as assessed by RT-PCR) show inhibition of constitutive Stat3 activation.

DN gp130 Inhibits EGF Receptor Signaling in Breast Cancer Cells. Signaling from EGFR family members, in addition to gp130 and Jak2 signaling, has been shown to support constitutive Stat3 activation in breast cancer cells (7–9). We verified these findings in

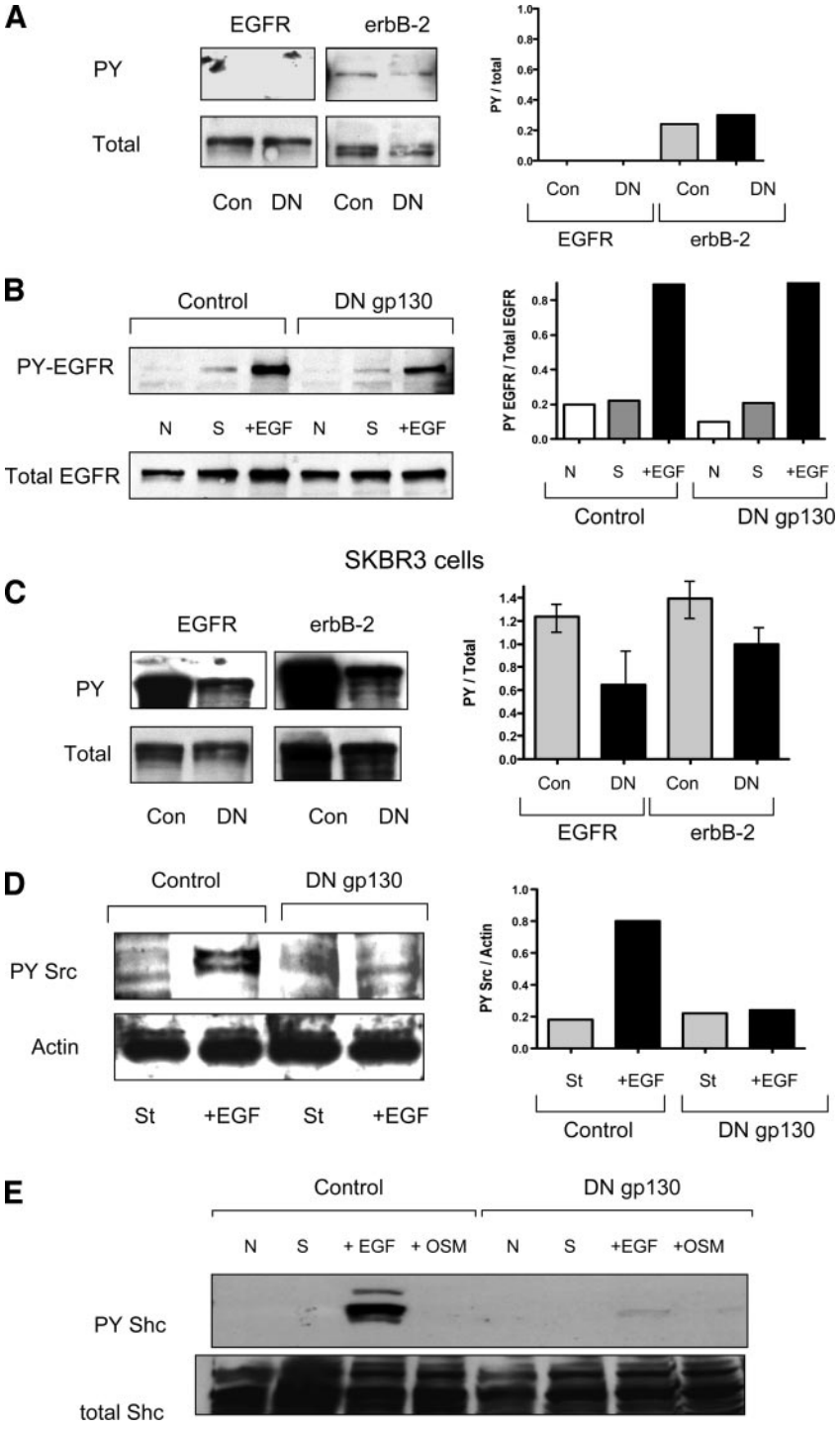

Fig. 6. Inhibition of gp130 results in down-regulation of EGF signaling pathways in MDA-231 breast cancer cells. *A.* MDA-231 single-cell clones expressing either DN gp130 (*DN*) or vector-only (*Con*) were lysed at 80% confluence. We used phosphospecific antibodies to detect constitutive activation of the EGFR and erbB-2. Blots were stripped and reblotted with total antibody to show equal loading. The *right panels* show densitometry analysis of the blots expressed as the ratio of PY staining to total receptor staining. Similar results were seen in two other experiments. *B.* MDA-231 clones expressing either vector-only control or DN gp130 were lysed at steady state growth (*N*), after overnight starvation in serum-free media (*S*), or after starvation and stimulation with EGF (10 ng/ml for 30 minutes). Lysates were immunoblotted with phosphospecific antibodies to EGFR. Blots were stripped and reblotted with total antibodies. The *right panels* show densitometry analysis of the blots expressed as the ratio of PY staining to total receptor staining. Similar results were seen in two other experiments. *C.* SKBR3 pools expressing either DN gp130 or vector-only controls were lysed at 80% confluence. We used phosphospecific antibodies to detect constitutive activation of the EGFR and erbB-2. Blots were stripped and reblotted with total antibody to show equal loading. The *right panels* show densitometry analysis of the cumulative results from three independent experiments; *bars*, ±SD. *D.* MDA-231 single-cell clones were starved and stimulated with EGF as in *D* above. Cell lysates were obtained and Src activation was assessed with a phosphospecific Src antibody. Blots were stripped and reblotted with antiactin to show equal loading. Densitometry analysis on the *right* shows the average results from two independent experiments. *E.* MDA-231 clones expressing either vector-only control or DN gp130 were lysed at steady state growth (*N*), after overnight starvation in serum-free media (*S*), or after starvation and stimulation with oncostatin M or EGF. Lysates were immunoblotted with phosphospecific antibodies to Shc. Blots were stripped and reblotted with total Shc antibodies.

our cells. Treatment of MDA-231 parental cells with AG1478, an inhibitor of EGFR kinase activity, results in marked decrease in EGF-induced EGFR and erbB-2 tyrosine phosphorylation (Fig. 5, *A* and *B*). Note that, in the absence of EGF stimulation, EGFR activation in MDA-231 cells is too low to be convincingly detected with phosphospecific antibodies (see Fig. 6*A*). Thus, we were unable to determine the effect of these inhibitors on basal EGFR signaling. In support of previous reports of the role of EGFR in constitutive Stat3 activation in breast cancer cells, treatment of MDA-231 parental cells with AG1478 results in decrease in constitutive Stat3 tyrosine phosphorylation (Fig. 5*C*).

Because of the importance of EGF signaling in constitutive Stat3 activation, and the known interaction of gp130 with EGFR family members in breast cancer and other cancers, we tested the effect of DN gp130 on EGFR signaling in breast cancer cells. The results of these experiments are shown in Fig. 6. MDA-231 cells lack detectable basal tyrosine phosphorylation of the EGFR, and have only a small amount of constitutive tyrosine phosphorylation of erbB-2 (Fig. 6*A*). DN gp130 has no effect on this low level of erbB-2 phosphorylation. We wondered if DN gp130 has an effect on EGFR activation (as reflected by tyrosine phosphorylation) in response to exogenously added EGF. As shown in Fig. 6*B*, there is no difference in EGFR activation by EGF in the presence of DN gp130. Similar results were seen with erbB-2 activation by EGF (data not shown). In contrast, SKBR3 cells (Fig. 6*C*) have marked constitutive phosphorylation of both receptors, via autocrine secretion by EGF family ligands (26). Expression of DN gp130 results in only modestly decreased EGFR and erbB-2 phosphorylation in SKBR3 cells (Fig. 6*C*). Our conclusion from these experiments is that expression of DN gp130 has no substantial effect on EGFR or erbB-2 activation (as reflected by tyrosine phosphorylation) in either MDA-231 or SKBR3 cells.

However, the ability of the phosphorylated EGFR to subsequently activate the downstream mediators Src and Shc is altered, as shown in Fig. 6, *D* and *E*. After EGF stimulation, the tyrosine phosphorylation of Src kinase is decreased in DN gp130-expressing MDA-231 cells (Fig. 6*D*). EGF-induced Src activation has been shown to phosphorylate and activate the adaptor protein Shc (27, 28). Shc tyrosine phosphorylation is markedly decreased in MDA-231 DN gp130 cells compared with control cells (Fig. 6*E*). We were unable to detect Shc activation in response to oncostatin M treatment in MDA-231 cells. These findings are consistent with the previously reported role of gp130 signaling on EGF activation of downstream adaptor molecules such as Shc and Grb2 (15). The effects of DN gp130 are specific for EGFR and gp130 signaling, because DN gp130 expression had no effect on IGF-1-induced total protein tyrosine phosphorylation, or on IGF-1-induced tyrosine phosphorylation of Shc in MDA-231 cells (data not shown).

Overall, our results show the ability of DN gp130 to inhibit signaling from multiple molecules known to cooperatively support constitutive Stat3 activation in cancer cells–EGFR, gp130, Jak2, and Src.

DN gp130 Expression in MDA-231 Cells Results in Decreased Malignancy *In vivo*. We used these characterized MDA-231 transfectants to test the effect of inhibition of gp130 signaling on the behavior of breast cancer cells *in vivo*. We used the orthotopic mammary fat pad injection model in nude mice. Table 1 shows the results of three experiments. We studied two independent clones each of MDA-231 cells expressing either DN gp130 or vector-only control. The animals receiving vector-only control MDA-231 cells had an overall engraftment rate of 72%. The tumors were large and bloody. Approximately 50% of the engrafted animals also had obvious metastatic disease. The metastatic sites included body wall, abdominal viscera, and, in several animals, copious carcinomatous ascites. The solid metastatic tumors were frequently as large as the primary tumors. (Note that metastatic disease was not included in Table 1; only the size of primary mammary tumors is presented).

Table 1 *Expression of DN gp130 is associated with decreased malignancy of MDA-231 cells in vivo*

	Engraftment (# with tumors/ # of injection sites)	Tumor size
MDA-231 vector-only	10/10 (clone 2A4)	$2{,}552 \pm 2{,}821$ mm^3
	5/10 (clone 1E12)	$1{,}250 \pm 1{,}074$ mm^3
	8/12 (clone 2A4)	$2{,}892 \pm 3{,}076$ mm^3
MDA-231 DN gp130	3/9 (clone 2A9)	472 ± 187 mm^3
	0/10 (clone 3D4)	
	2/10 (clone 2A9)	169 ± 205 mm^3

NOTE: Athymic nude mice received injection in the mammary fat pads with 1×10^6 cells of the indicated MDA-231 cell clones. Animals received injections in 1 to 2 mammary fat pads. Animals were sacrificed after 28 days. Tumors were removed, and tumor volume was measured. Several single-cell clones of both vector-only and DN gp130 were studied. Mean tumor size +/− SD is shown. Only measurable primary tumors were included in the calculations of mean tumor size.

The animals that received MDA-231 cells expressing DN gp130 had an engraftment rate of 18%. The tumors were small, white in color, round, and well circumscribed. There were no metastatic tumors noted in any of these animals.

The cumulative engraftment rates from these three experiments were as follows: control tumor % engraftment rate of 72% ± 25% and DN gp130 tumor % engraftment rate of 18% ± 17%. These values were significantly different ($P < 0.001$). The cumulative tumor size results from these three experiments were as follows: control tumors $2{,}231 \pm 866$ mm^3 and DN gp130 tumors 320 ± 214 mm^3. These were also significantly different ($P < 0.001$).

These *in vivo* results are particularly striking in light of the fact that DN gp130 cells grow faster than control cells *in vitro* (see Fig. 2). When non-necrotic orthotopic tumor areas are analyzed for apoptotic cells with TUNEL assay (Fig. 7*A*), there is no difference in apoptosis between control and DN gp130 cells. However, there is less mitotic activity in the DN gp130 tumors (Fig. 7*B*). We obtained similar results by using Ki-67 staining to detect dividing cells (data not shown).

MDA-231 Cells Expressing DN gp130 Have Decreased Angiogenic Activity *In vivo*. To reconcile the *in vitro* and *in vivo* results, we hypothesized that gp130 inhibition primarily affects invasiveness and/or angiogenesis *in vivo*, rather than growth. Immunohistochemical stains were used to determine the degree of angiogenesis in tumors obtained from the mammary fat pad experiments. Antibodies to the endothelial marker CD31 (PECAM) were used to detect endothelial cells (Fig. 7*C*). Tumors in the animals that received vector-only control cells had large areas of necrosis. Areas with viable tumor tissue showed profuse angiogenesis. The tumors from the animals that received DN gp130 expressing cells were devoid of angiogenesis. Similar histologic results were obtained in several other vector-only and DN gp130 tumors studied from two different experiments.

The Angiogenic Inhibitor TIMP-3 Is Up-Regulated in the Presence of DN gp130. We studied possible molecular mechanisms for the decreased invasion and angiogenesis of DN gp130 cells. There was no difference in vascular endothelial growth factor (VEGF), matrix metalloproteinase (MMP)-1, or MMP-9 protein expression by DN gp130 cells compared with vector-only cells (data not shown). However, the MMP/VEGF inhibitor TIMP-3 was up-regulated in the presence of DN gp130. TIMP-3 mRNA expression was increased in MDA-231 DN gp130 cells compared with controls (Fig. 7*D*). TIMP-3 protein was increased in whole cell lysates from both MDA-231 DN gp130 cells and T-47D DN gp130 breast cancer cells, compared with control cells (Fig. 7*E*). The nontumorigenic breast cancer cell line MCF-10A showed TIMP-3 protein expression level similar to the DN gp130 transfected cells (Fig. 7*E*). Additionally, as shown in Fig. 7*F*, there was marked TIMP-3 deposition in DN gp130 orthotopic tumors,

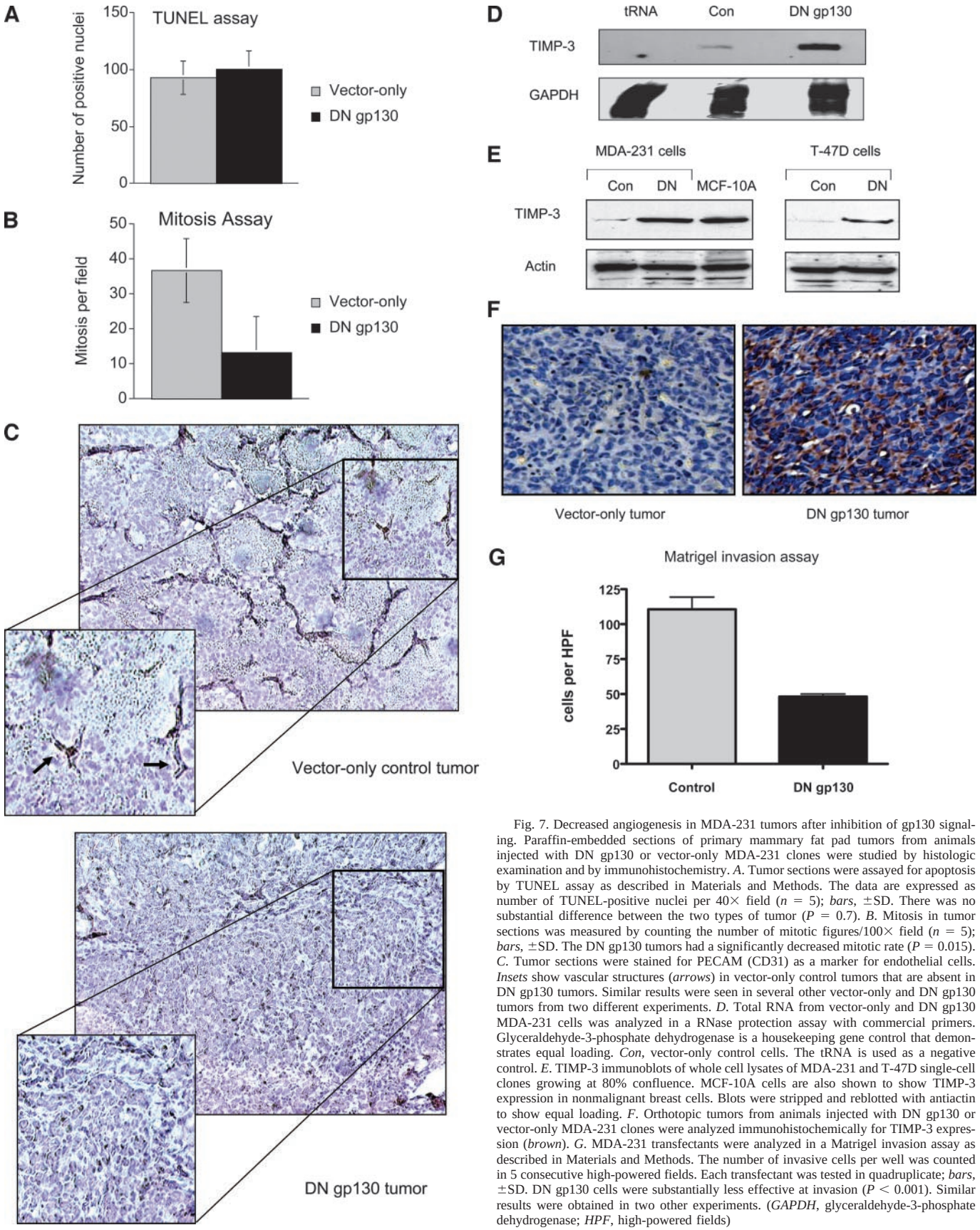

Fig. 7. Decreased angiogenesis in MDA-231 tumors after inhibition of gp130 signaling. Paraffin-embedded sections of primary mammary fat pad tumors from animals injected with DN gp130 or vector-only MDA-231 clones were studied by histologic examination and by immunohistochemistry. *A*. Tumor sections were assayed for apoptosis by TUNEL assay as described in Materials and Methods. The data are expressed as number of TUNEL-positive nuclei per 40× field ($n = 5$); *bars*, ±SD. There was no substantial difference between the two types of tumor ($P = 0.7$). *B*. Mitosis in tumor sections was measured by counting the number of mitotic figures/100× field ($n = 5$); *bars*, ±SD. The DN gp130 tumors had a significantly decreased mitotic rate ($P = 0.015$). *C*. Tumor sections were stained for PECAM (CD31) as a marker for endothelial cells. *Insets* show vascular structures (*arrows*) in vector-only control tumors that are absent in DN gp130 tumors. Similar results were seen in several other vector-only and DN gp130 tumors from two different experiments. *D*. Total RNA from vector-only and DN gp130 MDA-231 cells was analyzed in a RNase protection assay with commercial primers. Glyceraldehyde-3-phosphate dehydrogenase is a housekeeping gene control that demonstrates equal loading. *Con*, vector-only control cells. The tRNA is used as a negative control. *E*. TIMP-3 immunoblots of whole cell lysates of MDA-231 and T-47D single-cell clones growing at 80% confluence. MCF-10A cells are also shown to show TIMP-3 expression in nonmalignant breast cells. Blots were stripped and reblotted with antiactin to show equal loading. *F*. Orthotopic tumors from animals injected with DN gp130 or vector-only MDA-231 clones were analyzed immunohistochemically for TIMP-3 expression (*brown*). *G*. MDA-231 transfectants were analyzed in a Matrigel invasion assay as described in Materials and Methods. The number of invasive cells per well was counted in 5 consecutive high-powered fields. Each transfectant was tested in quadruplicate; *bars*, ±SD. DN gp130 cells were substantially less effective at invasion ($P < 0.001$). Similar results were obtained in two other experiments. (*GAPDH*, glyceraldehyde-3-phosphate dehydrogenase; *HPF*, high-powered fields)

compared with an absence of TIMP-3 protein in control tumors. Consistent with the elevated TIMP-3 expression in DN gp130 cells, matrigel invasion assays (Fig. 7*G*) showed decreased invasion of DN gp130 cells *in vitro*.

DISCUSSION

The goal of this work was to assess the effect of gp130 inhibition on breast cancer cells *in vitro* and *in vivo*. Thus, we developed and characterized genetically stable breast cancer cells lines expressing DN gp130. To our knowledge, this is the first demonstration of the effects of genetic inhibition of gp130 signaling in breast cancer cells *in vitro* or *in vivo*.

We elected to stably inhibit endogenous gp130 in breast cancer cell lines with a cytoplasmically truncated gp130. As predicted, this mutant gp130 was an effective dominant-negative inhibitor of IL-6 signaling in both COS-7 cells and Hep-G2 cells. The gp130 ligands bind very weakly, if at all, to gp130 alone (2). The primary ligand binding subunits of gp130 receptors are the specific α subunits rather than gp130. DN gp130 inhibits gp130 signaling by competition with endogenous cell surface gp130 for binding to other cell surface molecules, such as the IL-6R α, or the leukemia inhibitory factor receptor. In addition, DN gp130 likely competes with endogenous gp130 for interactions with EGFR family members. The interaction of cytokine receptors with other cytokine receptor subunits is mediated via extracellular and transmembrane domains. These domains are intact in DN gp130.

We found that expression of DN gp130 results in an increase in breast cancer cell growth *in vitro*. This finding was expected, because gp130 ligands such as oncostatin M (19), and IL-6 (15) have been reported to inhibit breast cancer cell growth. Presumably, DN gp130 inhibits a growth-suppressive autocrine gp130 signaling loop in MDA-231 and SKBR3 breast cancer cells. For instance, autocrine gp130 signaling in head and neck cancer (10) has been described previously. We did not additionally investigate the molecular mechanism of this growth stimulation by DN gp130. The significance of this result for the present work is for the interpretation of the animal experiments as discussed below.

A novel finding presented here is that dominant-negative inhibition of gp130 results in suppression of constitutive Stat3 activation in breast cancer cells. We found that DN gp130 inhibits signaling from both EGFR and gp130. This is a likely mechanism for the observed effects on Stat3, because both of these receptor pathways are known to be involved in constitutive Stat3 activation in breast cancer cells. DN gp130 inhibits endogenous gp130 by a straightforward dominant-negative mechanism. DN gp130 likely inhibits EGF family members through a similar dominant-negative mechanism. We propose that DN gp130 competes with endogenous gp130 for interaction with EGFR and erbB-2, and thus down-regulates EGFR/erbB-2 signaling. The gp130 has been shown to cooperate in EGFR activation (18), perhaps through recruitment of Jak kinases to the complex (15, 29). The inhibitory effects of DN gp130 results in decreased activation of the downstream signaling molecules Jak2 and c-Src. Both Jak2 and c-Src have been implicated in constitutive Stat3 activation in breast cancer cells (11).

Our data supports the hypothesis that constitutive Stat3 activation occurs in MDA-231 cells in the presence of very low (*i.e.*, below the level of detection with phosphotyrosine Western blots) constitutive signaling from gp130 and EGFR/erbB-2. This hypothesis is supported by the absence of constitutive Stat3 activation in the presence of chemical inhibition of EGFR (Fig. 5). Additionally, the fact that expression of DN gp130 increases the growth rate of MDA-231 cells (Fig. 2) is consistent with a low level of constitutive gp130 signaling. Low levels of any of the numerous potential gp130 and/or EGFR ligands could be present in FCS or secreted by the breast cancer cells in an autocrine manner (15, 30–32). Our hypothesis is also supported by the fact that MDA-231 cells show low levels of constitutive erbB-2 (Fig. 6*A*) and Jak2 (Fig. 3*C*) activation during steady state growth.

DN gp130 seems to have no effect on EGF ligand binding and subsequent autophosphorylation of the EGFR (Fig. 6). Rather, DN gp130 blocks the ability of endogenous wild-type gp130 to cooperate with the EGFR in the activation of downstream signaling molecules such as Src and Shc. This mechanism is consistent with the previously reported synergistic activity of gp130 in EGFR signaling in breast cancer (15).

The animal experiments reported here represent the first description of the effects of gp130 inhibition on breast cancer *in vivo*. Because of the variety of gp130 activities that have been reported in breast cancer cells *in vitro*, it was difficult to predict what effect inhibition of this receptor might have *in vivo*. For instance, intact signaling via gp130 has effects on breast cancer cells that would presumably lead to decreased malignancy, such as decreased growth, or increased differentiation (14). On the other hand, some of the reported gp130 ligand activities, such as activation of the oncogene Stat3 (3) and increased tumor cell motility (15), might be predicted to support increased malignancy.

We found that, despite a faster growth rate *in vitro*, MDA-231 cells with partial inhibition of gp130 signaling were much less malignant in the mammary fat pad animal model. This decreased growth seems to be a result of decreased angiogenesis and decreased local invasiveness. In the tumor-bearing animals, there was also a decreased mitotic rate in the DN gp130 cells compared with the vector-only cells (Fig. 7*B*). This seems at odds with the *in vitro* results of Fig. 2. This discrepancy probably reflects prolonged (28 days) growth in a microenvironment with poor blood flow (DN gp130 tumors) compared with growth in more adequate blood flow (vector-only cells). Different results may have been obtained if we had been able to study the tumors at earlier time points, such as a few days after injection (*i.e.*, DN gp130 might initially grow faster *in vivo*). Identifying and studying these very small tumors would be technically difficult, however, and was not attempted.

We found that TIMP-3 is up-regulated in the presence of DN gp130. TIMP-3 is an inhibitor of MMP (33) and VEGF activity (34) and is a potent inhibitor of tumor invasion and angiogenesis (35, 36). The decreased *in vitro* invasiveness of MDA-231 DN gp130 cells is consistent with increased TIMP-3 expression in these cells. TIMP-3 has strong binding affinity for tissue stroma. Thus, secreted TIMP-3 tends to become concentrated in the tumor stroma. This likely explains the marked difference in TIMP-3 protein detected in DN gp130 tumors compared with control tumors (Fig. 7*F*).

TIMP-3 has been shown previously to be down-regulated after activation of the EGFR (37) as well as gp130 and Stat3 (38, 39). We propose that TIMP-3 up-regulation after DN gp130 inhibition of EGFR and gp130 signaling provides a reasonable molecular mechanism for the animal results described here. The tumor stromal-bound TIMP-3 locally inhibits MMP and VEGF activity, blocking angiogenesis and local invasiveness.

Our observation of decreased local tumor growth in the presence of inhibition of gp130 suggests novel pharmacological approaches to the treatment of breast cancer. Several different methods of inhibition of gp130 signaling have been described that could be developed into drugs. Cytokine antagonists, such as the IL-6 superantagonist (40), and soluble gp130-IL-6Rα fusion proteins (21) have been developed. Another approach to gp130 inhibition would be immunotherapy with anti-gp130 (analogous to anti-erbB-2 therapy with Herceptin). An interesting oral compound called madindoline A has recently been

described that inhibits assembly of gp130 oligomeric signaling complexes (20). This drug inhibits IL-6 and IL-11 *in vivo*. Combination treatment with anti-EGF drugs might also increase the activity of gp130 inhibition *in vivo*. The dramatic effect of inhibition of gp130 on the *in vivo* behavior of breast cancer described here suggests that drugs such as those described above may have activity in this disease.

ACKNOWLEDGMENTS

The authors thank Dr. Stuart Frank for helpful suggestions and discussion and Dr. Catalina Suarez-Cuervo and Andrea Küster for technical assistance. Flow cytometry was done at the UAB Center for AIDS Research by Marion Spell.

REFERENCES

1. Peters M, Muller AM, Rose-John S. Interleukin-6 and soluble interleukin-6 receptor: direct stimulation of gp130 and hematopoiesis. Blood 1998;92:3495–504.
2. Taga T, Kishimoto T. Gp130 and the interleukin-6 family of cytokines. Annu Rev Immunol 1997;15:797–819.
3. Hirano T, Ishihara K, Hibi M. Roles of STAT3 in mediating the cell growth, differentiation and survival signals relayed through the IL-6 family of cytokine receptors. Oncogene 2000;19:2548–56.
4. Schindler CW. Series introduction. JAK-STAT signaling in human disease. J Clin Investig 2002;109:1133–7.
5. Bromberg JF, Wrzeszczynska MH, Devgan G, et al. Stat3 as an oncogene. Cell 1999;98:295–303.
6. Bromberg J. Stat proteins and oncogenesis. J Clin Investig 2002;109:1139–42.
7. Li L, Shaw PE. Autocrine-mediated activation of STAT3 correlates with cell proliferation in breast carcinoma lines. J Biol Chem 2002;277:17397–405.
8. Burke WM, Jin X, Lin HJ, et al. Inhibition of constitutively active Stat3 suppresses growth of human ovarian and breast cancer cells. Oncogene 2001;20:7925–34.
9. Ren Z, Schaefer TS. ErbB-2 activates Stat3 alpha in a Src- and JAK2-dependent manner. J Biol Chem 2002;277:38486–93.
10. Sriuranpong V, Park JI, Amornphimoltham P, et al. Epidermal growth factor receptor-independent constitutive activation of STAT3 in head and neck squamous cell carcinoma is mediated by the autocrine/paracrine stimulation of the interleukin 6/gp130 cytokine system. Cancer Res 2003;63:2948–56.
11. Garcia R, Bowman TL, Niu G, et al. Constitutive activation of Stat3 by the Src and JAK tyrosine kinases participates in growth regulation of human breast carcinoma cells. Oncogene 2001;20:2499–513.
12. Douglas AM, Goss GA, Sutherland RL, et al. Expression and function of members of the cytokine receptor superfamily on breast cancer cells. Oncogene 1997;14:661–9.
13. Karczewska A, Nawrocki S, Breborowicz D, Filas V, Mackiewicz A. Expression of interleukin-6, interleukin-6 receptor, and glycoprotein 130 correlates with good prognoses for patients with breast carcinoma. Cancer (Phila) 2000;88:2061–71.
14. Zhang F, Li C, Halfter H, Liu J. Delineating an oncostatin M-activated STAT3 signaling pathway that coordinates the expression of genes involved in cell cycle regulation and extracellular matrix deposition of MCF-7 cells. Oncogene 2003;22:894–905.
15. Badache A, Hynes NE. Interleukin 6 inhibits proliferation and, in cooperation with an epidermal growth factor receptor autocrine loop, increases migration of T47D breast cancer cells. Cancer Res 2001;61:383–91.
16. Tamm I, Kikuchi T, Cardinale I, Krueger JG. Cell-adhesion-disrupting action of interleukin 6 in human ductal breast carcinoma cells. Proc Natl Acad Sci USA 1994;91:3329–33.
17. Speirs V, Kerin MJ, Walton DS, et al. Direct activation of oestrogen receptor-alpha by interleukin-6 in primary cultures of breast cancer epithelial cells. Br J Cancer 2000;82:1312–6.
18. Qiu Y, Ravi L, Kung HJ. Requirement of ErbB2 for signalling by interleukin-6 in prostate carcinoma cells. Nature (Lond) 1998;393:83–5.
19. Grant SL, Hammacher A, Douglas AM, et al. An unexpected biochemical and functional interaction between gp130 and the EGF receptor family in breast cancer cells. Oncogene 2002;21:460–74.
20. Hayashi M, Rho MC, Enomoto A, et al. Suppression of bone resorption by madindoline A, a novel nonpeptide antagonist to gp130. Proc Natl Acad Sci USA 2002;99:14728–33.
21. Ancey C, Kuster A, Haan S, et al. Fusion protein of the gp130 and interleukin-6Ralpha ligand-binding domains acts as a potent interleukin-6 inhibitor. J Biol Chem 2003;278:16968–72.
22. Warri AM, Huovinen RL, Laine AM, Martikainen PM, Harkonen PL. Apoptosis in toremifene-induced growth inhibition of human breast cancer cells in vivo and in vitro. J Natl Cancer Inst (Bethesda) 1993;85:1412–8.
23. Sheibani N, Frazier WA. Thrombospondin-1, PECAM-1, and regulation of angiogenesis. Histol Histopathol 1999;14:285–94.
24. Castell JV, Gomez-Lechon MJ, David M, et al. Interleukin-6 is the major regulator of acute phase protein synthesis in adult human hepatocytes. FEBS Lett 1989;242:237–9.
25. Wegenka UM, Buschmann J, Lutticken C, Heinrich PC, Horn F. Acute-phase response factor, a nuclear factor binding to acute-phase response elements, is rapidly activated by interleukin-6 at the posttranslational level. Mol Cell Biol 1993;13:276–88.
26. Alimandi M, Romano A, Curia MC, et al. Cooperative signaling of ErbB3 and ErbB2 in neoplastic transformation and human mammary carcinomas. Oncogene 1995;10:1813–21.
27. Kassenbrock CK, Hunter S, Garl P, Johnson GL, Anderson SM. Inhibition of Src family kinases blocks epidermal growth factor (EGF)-induced activation of Akt, phosphorylation of c-Cbl, and ubiquitination of the EGF receptor. J Biol Chem 2002;277:24967–75.
28. Sato K, Kimoto M, Kakumoto M, et al. Adaptor protein Shc undergoes translocation and mediates up-regulation of the tyrosine kinase c-Src in EGF-stimulated A431 cells. Genes Cells 2000;5:749–64.
29. Yamauchi T, Ueki K, Tobe K, et al. Tyrosine phosphorylation of the EGF receptor by the kinase Jak2 is induced by growth hormone. Nature (Lond) 1997;390:91–6.
30. Ethier SP. Growth factor synthesis and human breast cancer progression. J Natl Cancer Inst (Bethesda) 1995;87:964–73.
31. Nicholson KM, Streuli CH, Anderson NG. Autocrine signalling through erbB receptors promotes constitutive activation of protein kinase B/Akt in breast cancer cell lines. Breast Cancer Res Treat 2003;81:117–28.
32. Chiu JJ, Sgagias MK, Cowan KH. Interleukin 6 acts as a paracrine growth factor in human mammary carcinoma cell lines. Clin Cancer Res 1996;2:215–21.
33. Brew K, Dinakarpandian D, Nagase H. Tissue inhibitors of metalloproteinases: evolution, structure and function. Biochim Biophys Acta 2000;1477:267–83.
34. Qi JH, Ebrahem Q, Moore N, et al. A novel function for tissue inhibitor of metalloproteinases-3 (TIMP3): inhibition of angiogenesis by blockage of VEGF binding to VEGF receptor-2. Nat Med 2003;9:407–15.
35. Spurbeck WW, Ng CY, Strom TS, Vanin EF, Davidoff AM. Enforced expression of tissue inhibitor of matrix metalloproteinase-3 affects functional capillary morphogenesis and inhibits tumor growth in a murine tumor model. Blood 2002;100:3361–8.
36. Ma DH, Chen JI, Zhang F, Hwang DG, Chen JK. Inhibition of fibroblast-induced angiogenic phenotype of cultured endothelial cells by the overexpression of tissue inhibitor of metalloproteinase (TIMP)-3. J Biomed Sci 2003;10:526–34.
37. Andreu T, Beckers T, Thoenes E, Hilgard P, von Melchner H. Gene trapping identifies inhibitors of oncogenic transformation. The tissue inhibitor of metalloproteinases-3 (TIMP3) and collagen type I alpha2 (COL1A2) are epidermal growth factor-regulated growth repressors. J Biol Chem 1998;273:13848–54.
38. Li WQ, Dehnade F, Zafarullah M. Oncostatin M-induced matrix metalloproteinase and tissue inhibitor of metalloproteinase-3 genes expression in chondrocytes requires Janus kinase/STAT signaling pathway. J Immunol 2001;166:3491–8.
39. Gatsios P, Haubeck HD, Van de Leur E, et al. Oncostatin M differentially regulates tissue inhibitors of metalloproteinases TIMP-1 and TIMP-3 gene expression in human synovial lining cells. Eur J Biochem 1996;241:56–63.
40. Savino R, Ciapponi L, Lahm A, et al. Rational design of a receptor super-antagonist of human interleukin-6. EMBO J 1994;13:5863–70.